



**HAL**  
open science

## Dynamic Shock Wave-Induced Amorphous-to-Crystalline Switchable Phase Transition of Lithium Sulfate

A. Sivakumar, S. Sahaya Jude Dhas, Shubhadip Chakraborty, Raju Suresh Kumar, Abdulrahman Almansour, Natarajan Arumugam, S. A. Martin Britto Dhas

► **To cite this version:**

A. Sivakumar, S. Sahaya Jude Dhas, Shubhadip Chakraborty, Raju Suresh Kumar, Abdulrahman Almansour, et al.. Dynamic Shock Wave-Induced Amorphous-to-Crystalline Switchable Phase Transition of Lithium Sulfate. *Journal of Physical Chemistry C*, 2022, 126 (6), pp.3194-3201. 10.1021/acs.jpcc.1c09411 . hal-03629794

**HAL Id: hal-03629794**

**<https://hal.science/hal-03629794>**

Submitted on 6 May 2022

**HAL** is a multi-disciplinary open access archive for the deposit and dissemination of scientific research documents, whether they are published or not. The documents may come from teaching and research institutions in France or abroad, or from public or private research centers.

L'archive ouverte pluridisciplinaire **HAL**, est destinée au dépôt et à la diffusion de documents scientifiques de niveau recherche, publiés ou non, émanant des établissements d'enseignement et de recherche français ou étrangers, des laboratoires publics ou privés.



Distributed under a Creative Commons Attribution - NonCommercial 4.0 International License

1 **Dynamic Shock Wave Induced Amorphous to Crystalline Switchable Phase Transition of**  
2 **Lithium Sulfate**

3 A.Sivakumar<sup>1</sup>, S.Sahaya Jude Dhas<sup>2</sup>, Shubhadip Chakraborty<sup>3</sup>, Raju Suresh Kumar<sup>4</sup>,  
4 Abdulrahman I. Almansour<sup>4</sup>, Natarajan Arumugam<sup>4</sup>, S.A.Martin Britto Dhas<sup>1\*</sup>

5 <sup>1</sup>Shock Wave Research Laboratory, Department of Physics, Abdul Kalam Research Center,  
6 Sacred Heart College, Tirupattur, Vellore, Tamil Nadu, India – 635 601

7 <sup>2</sup>Department of Physics, Kings Engineering College, Sriperumbudur, Chennai, Tamilnadu, India  
8 - 602 117

9 <sup>3</sup>Institut de Physique de Rennes, UMR CNRS 6251, Université de Rennes 1, 35042 Rennes  
10 Cedex, France

11 <sup>4</sup>Department of Chemistry, College of Science, King Saud University, P.O. Box 2455, Riyadh,  
12 Saudi Arabia- 11451

13  
14 **Corresponding Author:** [martinbritto@shcetpt.edu](mailto:martinbritto@shcetpt.edu)

15 **Abstract**

16 In recent years, there have been significant efforts put forth by the materials science  
17 researchers to search for new phase – change materials especially possessing the caliber of  
18 influencing switchable phase changes i.e., from crystal – crystal and crystal – amorphous. Phase–  
19 change materials of such kind have attracted a tremendous demand for the technologically  
20 important applications such as current resistive memories and thermal energy storage. In the  
21 present article, the switchable phase transitions of amorphous – glassy - crystalline – amorphous  
22 occurring in the samples of lithium sulfate have been systematically experimented and  
23 demonstrated at dynamic shock wave loaded conditions of various counts of shock pulses. The  
24 shocked samples have been evaluated by the powder X-ray diffraction (PXRD), Ultraviolet  
25 Visible spectroscopy (UV-Vis) and Raman spectroscopy. Shock wave induced orientational  
26 order-disorder of the SO<sub>4</sub> tetrahedron and the positional disorders of the lithium atoms have led  
27 to the observed switchable phase transitions with respect to the number of shock pulses.

28 **Keywords:** Li<sub>2</sub>SO<sub>4</sub>, shock waves, switchable phase transition, orientational order-disorder,  
29 positional disorder

## 30 **Introduction**

31 Switchable crystallographic phase transitions always have the special position of creative  
32 interest in solid state materials due to their controllable structural formation and functional  
33 diversity as compared to the forward and backward irreversible solid state phase transitions. This  
34 phenomenon can be applied in various applications as found in pressure transmitters, molecular  
35 switches, resistive memories, etc. Moreover, studies on the reversible phase transition of crystals  
36 would further push forward the current level of understanding of the molecules and their  
37 structures with respect to temperature and pressure.<sup>1-4</sup> It is well known that pressure serves as a  
38 thermodynamic variable which induces various solid state phase transition routes such as crystal-  
39 crystal, crystal-amorphous and amorphous-crystal that are very much possible to be obtained in  
40 the laboratory conditions.<sup>5,6</sup> On the one hand, the majority of static high pressure experiments  
41 that have been carried out on materials have the potential to authenticate the occurrence of  
42 reversible crystallographic phase transition when pressure is released.<sup>7-10</sup> In recent years, studies  
43 on the impact of shock waves imposed on solids have gained remarkable attention attracting a lot  
44 of materials scientists due to the variety of changes observed in properties of materials such as  
45 phase transitions and deformations.<sup>11-14</sup> On the other hand, reversible crystallographic phase  
46 transition occurring at dynamic shock wave loaded conditions is quite an unexpected behavior as  
47 compared to the results of static high pressure compression experiments so that in-depth research  
48 is further required in order to get a systematic understanding of the shock wave induced  
49 reversible crystallographic phase transitions. Moreover, even though several thousands of shock  
50 wave induced irreversible phase transitions have been observed and reported over the past 100  
51 years of shock wave research in materials science<sup>11-14</sup>, it could be noted that there are not many  
52 reports available for the dynamic shock wave induced crystallographically reversible phase  
53 transitions in solid state. Reversible magnetic phase transitions and crystallographic phase  
54 transition behaviors at dynamic shock wave loaded conditions have been observed in a few  
55 recent publications.

56 It has been demonstrated that cobalt oxide (Co<sub>3</sub>O<sub>4</sub>) nano- crystalline particles undergo  
57 reversible magnetic phase transition from super-paramagnetic to paramagnetic nature<sup>15</sup> and Zinc

58 ferrite ( $\text{ZnFe}_2\text{O}_4$ ) nano-crystalline particles undergo paramagnetic to super-paramagnetic  
59 behavior with respect to the number of shock pulses.<sup>16</sup> Furthermore, potassium sulfate ( $\text{K}_2\text{SO}_4$ )  
60 crystal exhibits the reversible crystallographic phase transition (from orthorhombic to hexagonal)  
61 with respect to the number of shock pulses.<sup>17</sup> On this note, lithium sulfate has been scrutinized  
62 for the present investigation, considering the possible switching behavior between the  
63 crystallographic phases by the impact of shock waves since both the crystals belong to the family  
64 of divalent metal sulfate crystals ( $\text{A}_2\text{BO}_4$ ). In general, sulfate materials are used as a classical  
65 example of materials so as to be investigated for the phase transition behaviour subjecting to  
66 experiments involving high-pressure and temperature.<sup>18-20</sup> Most of the sulfate materials obey the  
67 first order phase transition caused by orientation order-disorder effect occurring at high-pressure  
68 and high temperature regions.<sup>18-20</sup> Hence, the present investigation on shock wave induced phase  
69 changes of  $\text{Li}_2\text{SO}_4$  has a strong research objective in academic level as well as industrial point of  
70 view. The title sample has five crystallographic structures such as  $\alpha$ ,  $\beta$ ,  $\gamma$ ,  $\delta$  and  $\epsilon$  wherein  $\beta$  -  
71  $\text{Li}_2\text{SO}_4$  belongs to the room temperature phase which is phase transformed to  $\alpha$ - $\text{Li}_2\text{SO}_4$  at 845 K  
72 and it is used as a solid electrolyte because of its outstanding electrical conductivity i.e.  
73 particularly  $\alpha$ - $\text{Li}_2\text{SO}_4$  and the remaining phases are represented as high-pressure phases.<sup>21-25</sup> Even  
74 though several publications are available for  $\text{Li}_2\text{SO}_4$  crystal on phase transitions occurring at  
75 high-pressure and high temperature conditions, to date, no one has reported the reversible  
76 amorphous –glassy - crystalline – amorphous phase transitions of  $\text{Li}_2\text{SO}_4$  sample.

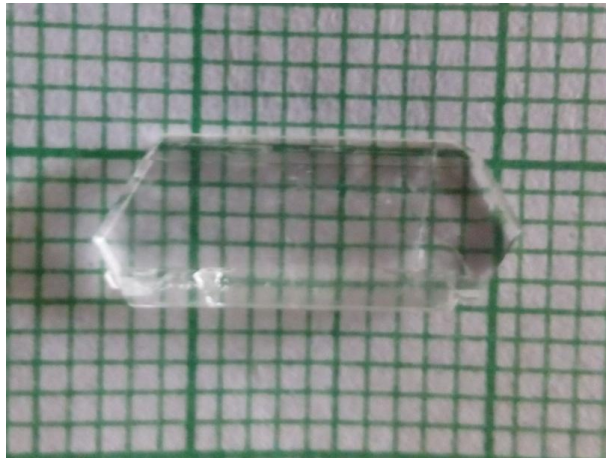
77 The present research article is aimed at demonstrating the reversible crystallographic  
78 phase transition with respect to the number of shock pulses as it has been already witnessed for  
79 potassium sulfate crystal.<sup>17</sup> Since shock wave induced reversible phase transition is very fast and  
80 cost effective, such kind of experiments may bring about a systematic methodology with which it  
81 would be possible to induce the reversible phase transition in potential materials such that a lot of  
82 insights could be derived. On those lines, many of the requirements which are based on phase –  
83 change materials can be fulfilled for the scientific world as well as industrial applications.

84

85

## 86 **Experimental methodology**

87 In this study, Lithium sulfate ( $\text{Li}_2\text{SO}_4$ ) samples were obtained by employing the  
88 conventional slow evaporation method. Commercially available  $\text{Li}_2\text{SO}_4$  (98.5%) was bought  
89 from Sigma Aldrich and was used without further purification for the growth process. The  
90 saturated solution of  $\text{Li}_2\text{SO}_4$  was prepared by dissolving it in double distilled water. The solution  
91 was stirred continuously for 5 hours with the help of a magnetic stirrer in order to completely  
92 dissolve  $\text{Li}_2\text{SO}_4$  which was filtered into a beaker. The solution was kept undisturbed for the  
93 crystallization. After 34 days, an optically transparent specimen with the dimension of  $14 \times 6 \times 1$   
94  $\text{mm}^3$  was obtained as shown in Fig.1.



95

96

Fig.1 As grown  $\text{Li}_2\text{SO}_4$  specimen by the slow evaporation method

97

98 In total, four identical samples (1mm thickness) have been cut and polished maintaining a  
99 high quality. Before beginning the shock wave loading experiment, it has been confirmed that all  
100 the four samples belong to the amorphous state. Among the four samples, one sample has been  
101 kept as the control while the other three samples have been utilized for the respective 1<sup>st</sup>, 2<sup>nd</sup>, and  
102 3<sup>rd</sup> shocked conditions which means that for the first sample, one shock pulse has been applied  
103 while for the second sample, two shock pulses have been applied and for the 3<sup>rd</sup> sample, three  
104 shock pulses have been exposed. In the present investigation, a shock wave of Mach number 2.2  
105 is utilized that has the transient pressure of 2.0 MPa and temperature 864 K. The shock waves  
106 have been generated by an in-house tabletop pressure driven shock tube (Reddy tube). The  
shock tube has three sections such as driver, driven and diaphragm sections which are made of

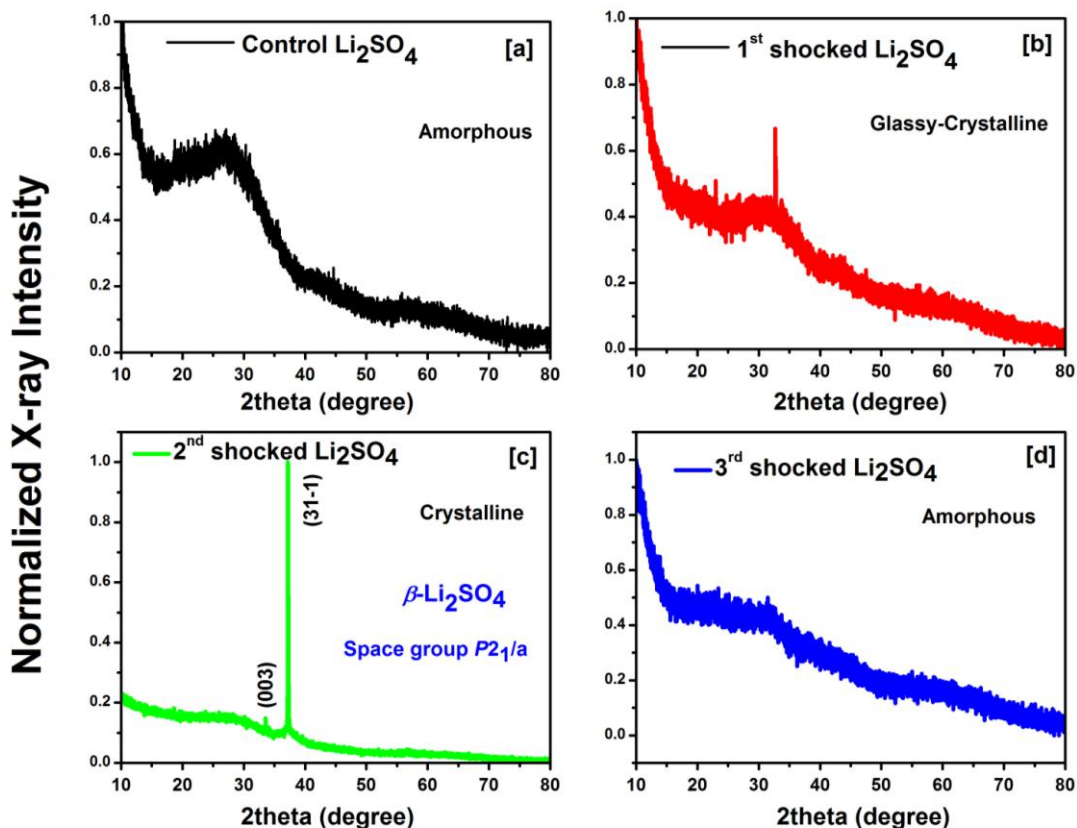
107 seamless steel. The driver and driven sections consist of long tubes of 48 cm and 180 cm,  
108 respectively and both have 1.5 cm of inner diameter with the wall thickness of 3mm and the  
109 atmospheric air is used as the input source for the required shock wave generation. The working  
110 methodology of the shock tube and the loading process have been detailed in our previous  
111 publications.<sup>14,15</sup>

112 The shock wave loaded samples have been further investigated using a powder  
113 XRD (Rigaku - SmartLab X-Ray Diffractometer, Japan in which Cu K $\alpha$  has been used as the X-  
114 ray source,  $\lambda=1.5407$  Å) and UV-Vis spectroscopy (with a varian Cary 5E UV – Visible  
115 spectrometer between 200 and 800 nm). Raman spectrometry (LabRAM HR Evolution, France)  
116 has been employed to understand the phase details of the test materials over the wavenumber  
117 region of  $100^{-1}$  to  $1300$   $\text{cm}^{-1}$  with the laser source of wavelength 532 nm.

## 118 **Results and Discussion**

### 119 **Structural properties of Li<sub>2</sub>SO<sub>4</sub> samples**

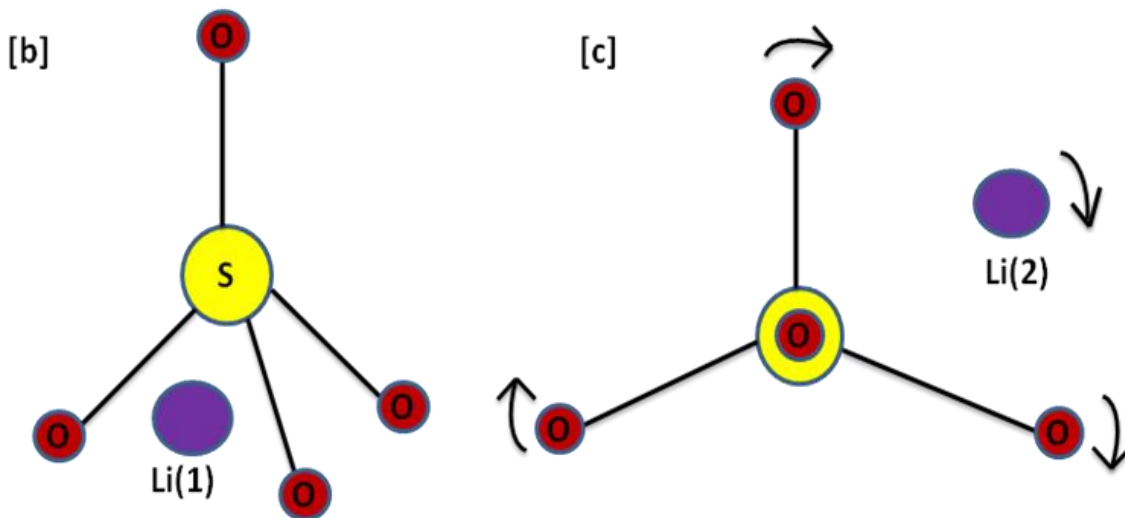
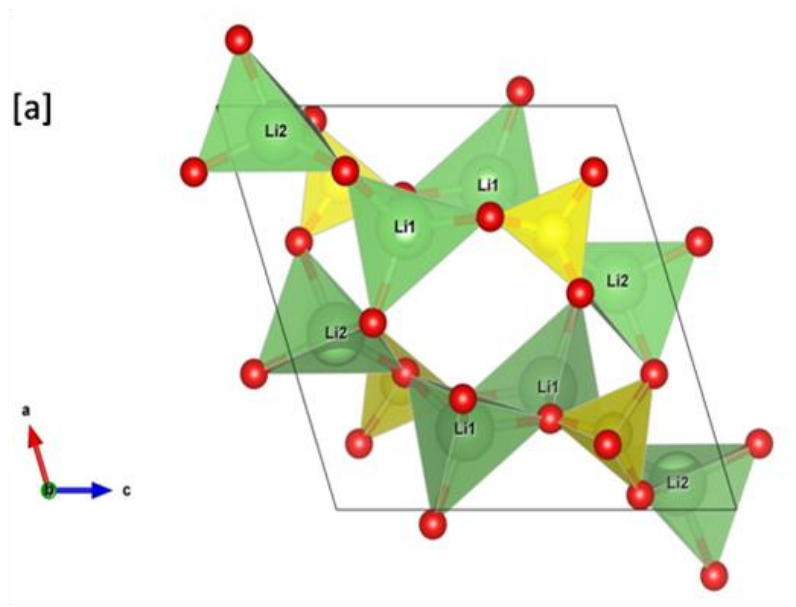
120 The diffraction patterns of the control and the shock exposed Li<sub>2</sub>SO<sub>4</sub> samples are  
121 presented in Fig.2 (a-d). The control sample looks well-shaped and transparent; however, the X-  
122 ray diffraction study reveals that the sample is in amorphous nature (Fig.2a). In general,  
123 particularly for Li<sub>2</sub>SO<sub>4</sub>, it is a critical task for the crystal growers to grow a good quality single  
124 crystal with the monoclinic phase due to the discontinuous changes occurring for Li atoms in the  
125 tetrahedral site which may induce a large number of improper locations for Li atoms in the  
126 crystal lattice.<sup>24-28</sup>



127

128 Fig.2 Powder XRD profiles of the control and shocked  $\text{Li}_2\text{SO}_4$  (a) the control, (b) 1<sup>st</sup> shocked  
 129 (c) 2<sup>nd</sup> shocked (c) 3<sup>rd</sup> shocked samples

130 Moreover, the test sample has two lithium atoms such as Li (1) and Li (2) bonded with  
 131 oxygen atoms. Among these two atoms, Li (1) atom is static while Li (2) is mobile and  $\text{SO}_4$   
 132 tetrahedral is coordinated with Li atoms. Due to its mobile nature, Li (2) and  $\text{SO}_4$  orientation may  
 133 generate positional disorder along with orientational disorder and the corresponding schematic  
 134 diagram is presented in Fig.3. As per the crystallographic structures of the test sample,  $\text{Li}^+$  ions  
 135 have three different lattice sites such as  $\frac{1}{4}$ ,  $\frac{1}{4}$ ,  $\frac{1}{4}$ ,  $\frac{1}{2}$ ,  $\frac{1}{2}$ ,  $\frac{1}{2}$  and  $\frac{3}{4}$ ,  $\frac{3}{4}$ ,  $\frac{3}{4}$ . Among the listed lattice  
 136 sites,  $\frac{1}{4}$ ,  $\frac{1}{4}$ ,  $\frac{1}{4}$  provides too small space whereas  $\frac{1}{2}$ ,  $\frac{1}{2}$ ,  $\frac{1}{2}$  and  $\frac{3}{4}$ ,  $\frac{3}{4}$ ,  $\frac{3}{4}$  provide too large  
 137 space.<sup>26,27</sup> However,  $\text{Li}^+$  (1) ions are occupied in the tetrahedral site quiet easily compared to  $\text{Li}^+$   
 138 (2) site due to the different lattice site sizes. On the other hand, the test sample has two lithium  
 139 atoms in the structure which are non-equivalent to the symmetric operation. Moreover, among  
 140 the two lithium atoms, one (Li-1) is static and the second (Li-2) is mobile.<sup>27,28</sup>



141

142

Fig.3 (a) Crystal packing of  $\beta$ -Li<sub>2</sub>SO<sub>4</sub> (b) Li(1)-SO<sub>4</sub> (c) Li(2) –SO<sub>4</sub>

143

144

145

146

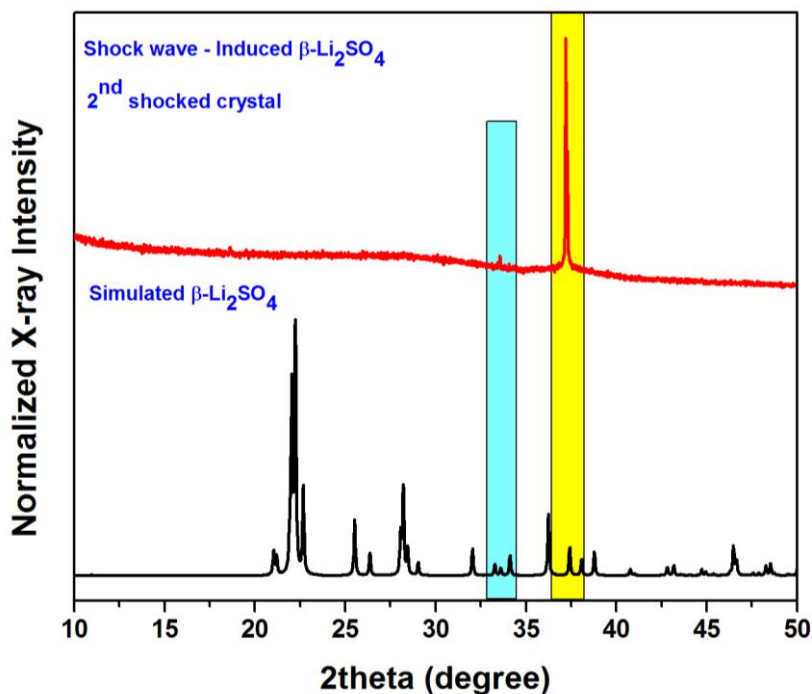
147

148

149

Due to the mobile nature of Li (2) atom, the interaction between the Li (2) and oxygen atom is significantly reduced so that the lattice disorder enhances. Hence, it leads to the amorphization during the crystal growth.<sup>25, 26</sup> At the first shocked condition, the corresponding XRD profile (Fig. 2b) shows a low intensity peak at 32.5° which does not match with either  $\alpha$  or  $\beta$  or else with any other high-pressure phases so that it is considered as a glassy material.<sup>29</sup> Moreover, such kind of a crystal with this phase may be called as plastic crystal. The XRD profile of the test sample obtained upon the exposure of 2<sup>nd</sup> shock wave is presented in Fig. 2c.

150 Tiny and intense crystalline peaks are observed at 33.4° and 37.2°. The observed crystalline peak  
151 positions match well with the simulated peak position of  $\beta$ -Li<sub>2</sub>SO<sub>4</sub> as shown in Fig.4.



152

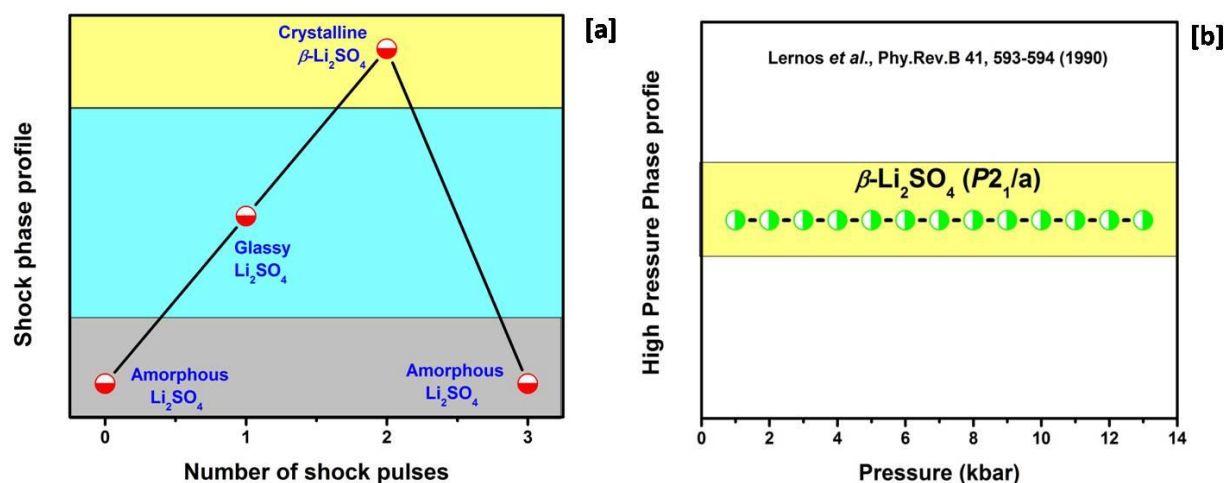
153 Fig.4 Powder-XRD patterns of simulated and shock induced  $\beta$ -Li<sub>2</sub>SO<sub>4</sub>

154 The applied 2<sup>nd</sup> shock wave has induced a phase transition from amorphous to crystalline  
155 for the test sample via glassy phase at 1<sup>st</sup> shocked condition. From the literature, it is noted that  
156  $\beta$  to  $\alpha$  - Li<sub>2</sub>SO<sub>4</sub> phase transition is due to the enhancement of the orientational disorder of SO<sub>4</sub>  
157 tetrahedron.<sup>21-26</sup> On the other hand, the results of several high-pressure and high temperature  
158 experiments have revealed that SO<sub>4</sub> tetrahedron plays a major role in the phase transitions of  
159 crystalline to amorphous and vice versa.<sup>30</sup> In the case of the cationic LiO<sub>4</sub>, the tetrahedra has 14  
160 times higher compressibility than that of the anionic SO<sub>4</sub> tetrahedra.<sup>18,21</sup> At shocked conditions,  
161 deformation of the LiO<sub>4</sub> tetrahedra might have taken place, whereas the SO<sub>4</sub> groups are expected  
162 to undergo tilting which plays a key role in the order-disorder process.<sup>18,21</sup> At shocked  
163 conditions, the tilting angle of the SO<sub>4</sub> tetrahedron changes with respect to the number of shock  
164 waves such that the Li<sup>+</sup> ions' atomic sites, especially Li(2) is changed due to the existence of  
165 positional disorder caused by the impact of shock waves. As per the reported phase transition

166 studies, it could be suggested that during the shock wave loaded condition, orientational order of  
167 the  $\text{SO}_4$  tetrahedron with static and mobile lithium atoms might have appeared during the second  
168 shock wave loaded condition.<sup>25, 31,32</sup> The bond angles between lithium and oxygen atoms of O-  
169 Li(1)-O is  $106.5\text{-}115.2^\circ$  and O-Li(2)-O is  $88.6\text{-}124.5^\circ$ . Due to the presence of wider angle, Li(2)  
170 has undergone maximum deformation level. Moreover, the bond energies of Li-O and S-O are  
171  $333.5 (\pm 8.4)$  and  $110 \text{ kJmol}^{-1}$ , respectively which makes the  $\text{SO}_4$  tetrahedra less stable compared  
172 to the  $\text{LiO}_4$  tetrahedron. In addition to that, the applied shock waves may supply the sufficient  
173 latent heat to crystallize the glassy phase of  $\text{Li}_2\text{SO}_4$  which can be called as shock wave induced  
174 dynamic re-crystallization.<sup>17</sup> As seen in Fig.4,  $\beta$  - phase of the test sample's standard powder  
175 XRD pattern has several diffraction peaks appearing between 20 and 50 degree. But, the  
176 observed shocked crystal's XRD profile shows the strong diffraction peak (31-1) and a tiny  
177 diffraction peak (300) which confirms that the phase transition has occurred at the 2<sup>nd</sup> shocked  
178 condition.

179 Furthermore, the 3<sup>rd</sup> shock wave loading process has been enabled for the test sample in  
180 such a way that XRD measurement could make a clear phase diagram of  $\text{Li}_2\text{SO}_4$  specimen with  
181 respect to the number of shock pulse. It has been strongly expected that the XRD pattern would  
182 provide the high-pressure phase of the test sample ( $\alpha\text{-Li}_2\text{SO}_4$ ) as exhibited by potassium  
183 sulfate.<sup>17</sup> On the other hand, it has been a surprise to observe the amorphous nature of  $\text{Li}_2\text{SO}_4$   
184 specimen at the 3<sup>rd</sup> shock wave loaded condition as reflected by the disappearance of diffraction  
185 peaks in the XRD pattern. The corresponding XRD profile is presented in Fig.2d. In this context,  
186 the orientational – disorder of the  $\text{SO}_4$  tetrahedron plays a significant part to initiate and enable  
187 the crystalline - amorphous phase transition. Since the  $\text{SO}_4$  tetrahedron is absolutely free for the  
188 rotation, it could enforce the orientational – disorder behavior at shock wave loaded conditions.<sup>17</sup>  
189 At the 3<sup>rd</sup> shock wave loaded condition, the thermodynamic barrier of the system and the critical  
190 phase transition region could have experienced break-down because of the higher transient  
191 pressure and temperature so that the test sample might have undergone the process of complete  
192 atomic disorder. The lattice symmetry of  $\text{Li}_2\text{SO}_4$  is completely broken at the 3<sup>rd</sup> shock wave  
193 paving the way for the crystalline – amorphous phase transition. On the other hand, Li(2) sites  
194 might have experienced the positional disorder occurring at this stage that could have stimulated  
195 the shock wave induced amorphization of  $\text{Li}_2\text{SO}_4$ . It is worthwhile to note that the control and

196 the 3<sup>rd</sup> shocked test samples have the amorphous nature which confirms that the test sample has  
 197 undergone the reversible amorphization phase transition via glassy phase and crystalline phase  
 198 by the influence of the shock waves. The shocked phase-profile of the test sample with respect to  
 199 the number of shocks is presented in Fig.5a and the static pressure compression phase profile of  
 200 the material is displayed in Fig.5b [20].



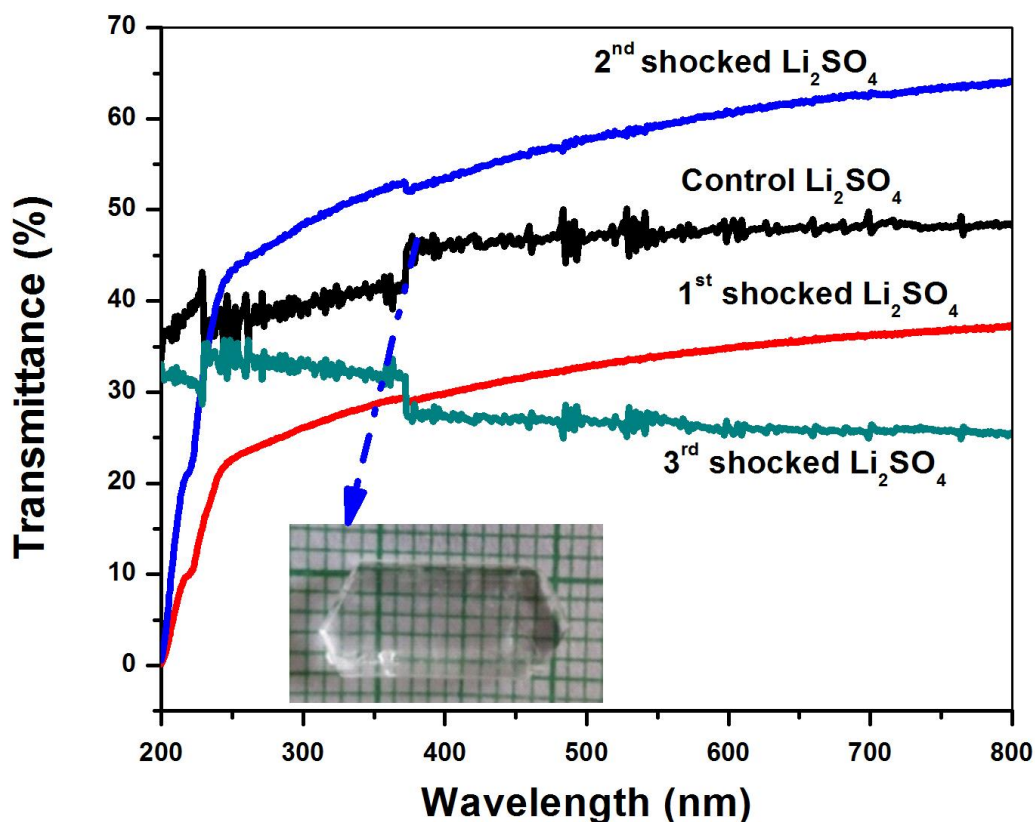
201

202 Fig.5 (a) Schematic shocked phase-profile of the control and shocked  $\text{Li}_2\text{SO}_4$  samples (b)

203 Static pressure compression phase profile of  $\beta\text{-Li}_2\text{SO}_4$  [20]

#### 204 UV-Visible spectroscopic studies

205 For optically transparent materials, UV – Vis spectroscopic analysis is one of the prime  
 206 studies to understand the electronic structure and optical properties. In Fig 6, the observed optical  
 207 transmittance spectra of the control and the shocked test samples are reported. The absence of  
 208 characteristic absorption peak in Fig. 6 for the control sample is one of the evidences of its  
 209 amorphous nature.<sup>33,34</sup> At the 1<sup>st</sup> shocked condition, the test sample shows the absorption band  
 210 edge at 243 nm and it exhibits 37% optical transmittance at 800 nm. At shocked condition, the  
 211 appearance of absorption band edge for the 1<sup>st</sup> shocked sample is due to the phase transition from  
 212 amorphous – glassy phase.



213

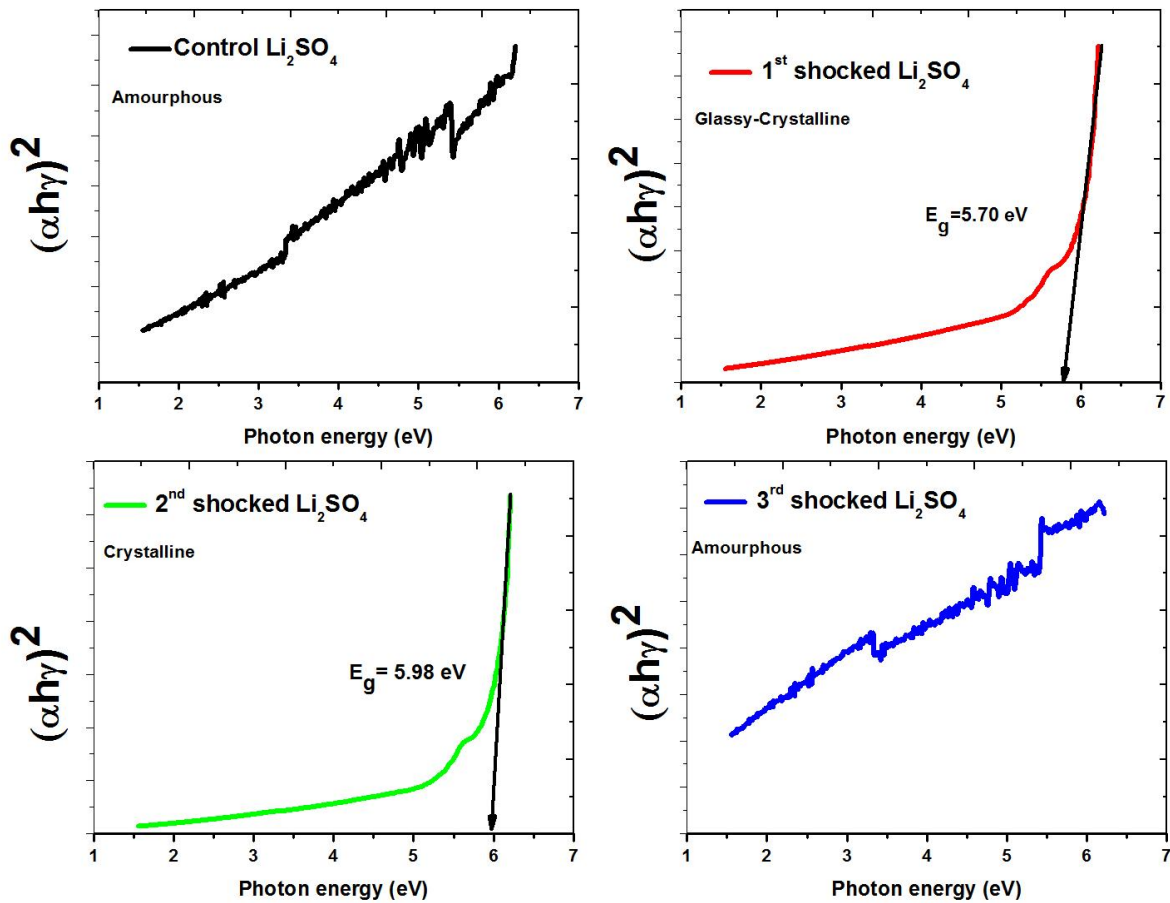
214 Fig.6 Optical transmittance spectra of the control and shock exposed  $\text{Li}_2\text{SO}_4$

215 At the second shocked condition, the test sample's absorption band edge of the test  
 216 sample has got shifted towards the lower wavelength and the optical transmittance has  
 217 significantly increased from 37 % to 64 % at 800 nm. These two factors give rise to the  
 218 considerable authentication for the phase transition occurring due to the shock wave induced  
 219 orientational disorder-order process which might have led to the changes in optical transmittance  
 220 for the test sample. It has been observed similar changes in the  $\alpha$ -phase of potassium sulfate  
 221 crystal which undergoes red shift resulting to lower optical transmittance than that of  $\beta$ -phase at  
 222 shock wave loaded condition.<sup>17</sup> Making a comparison, it can be represented that the glassy phase  
 223 has a partial disorder phase as against the  $\beta$ -phase of  $\text{Li}_2\text{SO}_4$ . Hence, it has lower optical  
 224 transmittance than that of  $\beta$ -phase of  $\text{Li}_2\text{SO}_4$ . Furthermore, after the 3<sup>rd</sup> shock, the crystal  
 225 showcases the optical transmittance spectrum similar to the control sample with slight changes in

226 terms of optical transmittance percentage and shape of the pattern. Hence, it confirms  
227 categorically that the test sample has undergone the amorphous nature because of the  
228 disappearance of orientational order of  $\beta$ -phase of  $\text{Li}_2\text{SO}_4$  by the impulsion of shock waves. It  
229 could be noted that the results of structural and optical transmittance are found to be well  
230 matched with respect to the number of shock pulse which clearly indicates the reproducibility of  
231 the unprecedented results at shocked conditions.

232 In Fig. 7, the optical band gap energies of the control and shock exposed samples are  
233 presented as calculated by classical Tauc plot.<sup>35</sup> As it is known from the XRD and optical  
234 transmittance measurements, the control  $\text{Li}_2\text{SO}_4$  has the amorphous nature so that it is not  
235 possible to calculate the band gap energy for the control sample. Moreover, the values of  
236 absorption coefficient are not satisfied for Tauc plot so that it is not possible to find the band gap  
237 energy. Hence, it is confirmed that the control sample has high electrical resistant behavior.  
238 Moreover, the absence of lithium ions ( $\text{Li}_2$ ) in the tetrahedral position is the major reason behind  
239 the high electrical resistance. The initial phase of the amorphous nature is represented as the  
240 RESET phase since it has a very high resistivity.

241 At the 1<sup>st</sup> and 2<sup>nd</sup> shocked conditions, the direct band gap energies are observed to be 5.70  
242 and 5.98 eV, respectively. From the obtained values, it is clear that the crystalline samples have  
243 higher values of band gap energy than that of the glassy phase. Hence, the crystalline sample has  
244 lower electrical conductivity than the glassy phase. So far, numerous researchers have reported  
245 the electrical conductivity of the test sample based on their phases and found that  $\alpha$ - $\text{Li}_2\text{SO}_4$  has  
246 higher electrical conductivity than that of the  $\beta$ - $\text{Li}_2\text{SO}_4$  due to the rotor type phase based on the  
247 peddle wheel and percolation mechanism.<sup>27,28,36,37</sup> From the available literature reports, there  
248 could be two prominent reasons behind the changes in electrical conductivity observed for the  
249 order and the disordered phases. Firstly,  $\beta$ - $\text{Li}_2\text{SO}_4$  is the ordered phase such that the rotational  
250 freedom of the  $\text{SO}_4$  tetrahedron is quite lower than that of the disordered phase. Hence, the  
251 mobility of the lithium ions is low so that it has low electrical conductivity. Secondly in the case  
252 of  $\beta$ - $\text{Li}_2\text{SO}_4$  phase, interaction of the lithium and oxygen atoms is quite low because of the higher  
253 bond length. Hence, the crystalline phase has lower electrical conductivity than that of the glassy  
254 phase.



255

256

Fig.7 Band-gap energy of the control and shocked  $\text{Li}_2\text{SO}_4$

257

258

259

260

261

The crystalline phase can be represented as the SET phase due to the conduction behavior. At the 3<sup>rd</sup> shock, the disappearance of the crystalline phase and the appearance of the amorphous nature occur and as per Tauc plot, it exhibits the similar results when compared to the control test sample. Hence, again it comes to the RESET phase. Such kind of SET and RESET reversible phase changing materials are highly used in sensors.<sup>38,39</sup>

262

263

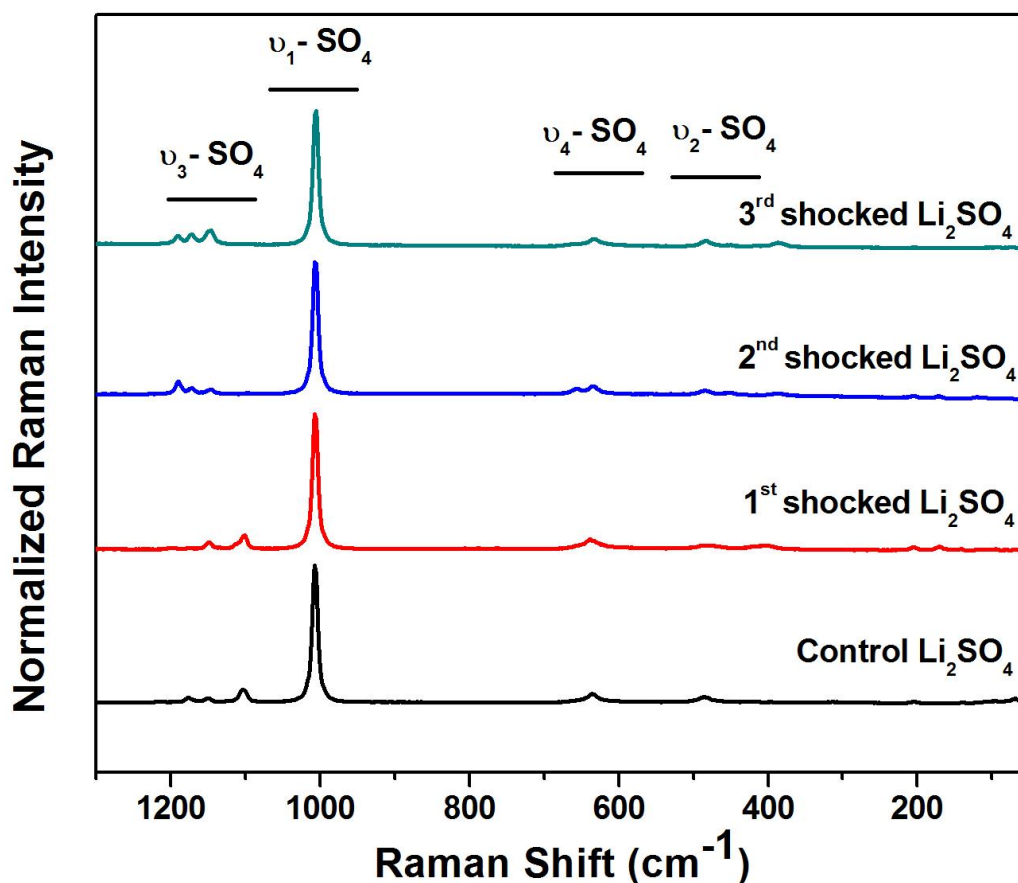
264

265

266 **Raman Spectral Analysis**

267 As seen in Fig.8, the normal Raman bands of  $\text{Li}_2\text{SO}_4$  are observed at 484, 634, 1007 and  
268  $1103\text{ cm}^{-1}$  in the control sample for the respective  $\nu_2$ ,  $\nu_4$ ,  $\nu_1$  and  $\nu_3$   $\text{SO}_4$  vibration bands. As per  
269 the previous reports of  $\beta\text{-Li}_2\text{SO}_4$ ,<sup>40-43</sup> the  $\text{SO}_4$  of  $\nu_2$ , and  $\nu_4$  double degenerate Raman bands and  
270 one lithium Raman lattice mode should have evolved at  $385$  or  $362\text{ cm}^{-1}$ .<sup>40,41</sup>

271

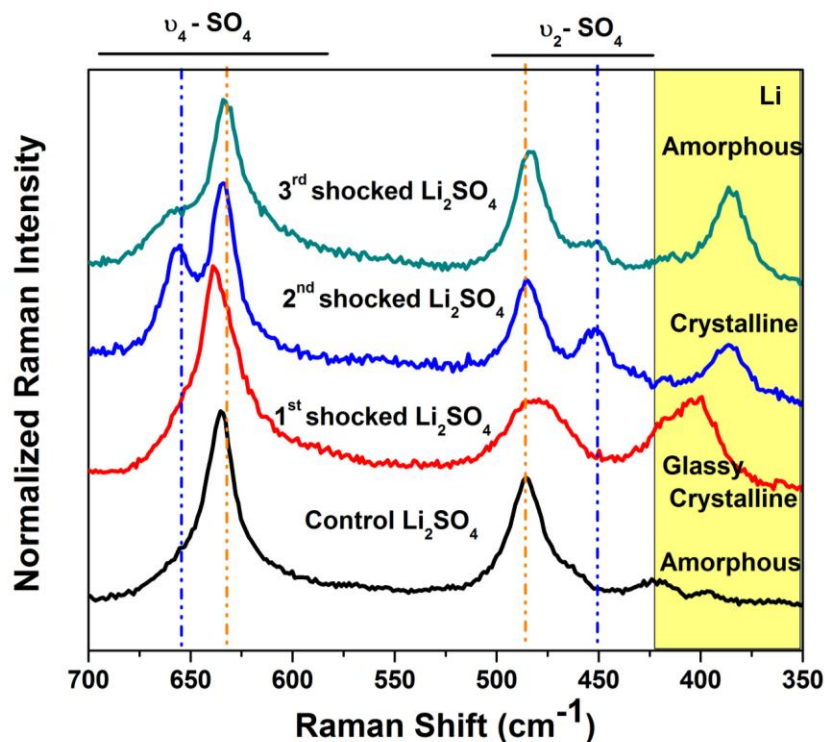


272

273 Fig.8 Raman spectra of the control and shocked  $\text{Li}_2\text{SO}_4$

274 But, such kinds of characteristics Raman bands of  $\beta\text{-Li}_2\text{SO}_4$  are completely not visible. It  
275 may be due to the formation of positional disorder of lithium atoms and rotational disorder of  
276  $\text{SO}_4$  tetrahedral. Hence, due to such kind of defects and disorders, the control sample might have  
277 the amorphous nature which is very well corroborated with the results of XRD and UV-Visible

278 studies. At shocked conditions, the normal  $\text{SO}_4$  Raman bands are not significantly altered. But,  
 279 in the case of characteristic Raman band positions, considerable changes have been observed.  
 280 The Raman band of  $\nu_3$  region has also undergone significant changes whereas the Raman bands  
 281 of  $\nu_2$ , and  $\nu_4$  are highly coupled with lithium atoms. Hence, it is worthwhile to investigate more  
 282 on these two Raman bands so that, for better visibility of such changes, the zoomed-in versions  
 283 of the prominent region of Raman bands ( $\nu_2$ , and  $\nu_4$ ) of the control and shocked samples are  
 284 provided in Fig.9.



285  
 286 Fig.9 Zoomed-in versions of Raman spectra of the control and shocked  $\text{Li}_2\text{SO}_4$  ( $350\text{-}700\text{ cm}^{-1}$ )  
 287 As seen in Fig.9, at the 1<sup>st</sup> shocked condition, the normal  $\nu_4$  and  $\nu_2$  bands are reproduced  
 288 with a very little Raman shift whereas a new Raman band appears at  $399\text{ cm}^{-1}$ . As per the  
 289 previous reports, this particular Raman band belongs to lattice mode of lithium ion for the  
 290 ambient crystalline phase which indicates the reduction of net degree of positional disorder of  
 291 lithium atoms reflecting the formation of the glass-crystalline nature of  $\text{Li}_2\text{SO}_4$ . Moreover, the  
 292 presence of single band at  $\nu_4$  and  $\nu_2$  regions support that the sample is not still crystalline.<sup>40,41</sup>

293 Surprisingly, at the 2<sup>nd</sup> shocked condition, the singlet SO<sub>4</sub> Raman bands of  $\nu_4$  and  $\nu_2$  are  
294 completely converted as doublet. Furthermore, the lithium Raman band is shifted from 399 to  
295 385 cm<sup>-1</sup> and this position is found to be well matched with Bg polarization of lattice lithium  
296 mode.<sup>40, 41</sup> The Raman spectrum of the 2<sup>nd</sup> shocked condition well corroborate with  $\beta$ -Li<sub>2</sub>SO<sub>4</sub>  
297 which demonstrates the crystalline nature of the test sample because of the rapid reduction of  
298 positional disorder and rotational disorder of SO<sub>4</sub>. In addition to that, at the 3<sup>rd</sup> shocked  
299 condition, the lithium Raman band position is not altered. But the doublet Raman bands at  $\nu_4$  and  
300  $\nu_2$  regions become singlet that indicates the enhancement of rotational disorder of the SO<sub>4</sub>  
301 tetrahedral which leads to the amorphous nature of the test sample. Note that, in the case of  
302 dynamic shocked conditions and high-pressure compression conditions, SO<sub>4</sub> anionic units are  
303 found to have undergone significant rotational order-disorder effects and such results have been  
304 well documented.<sup>44 - 47</sup>

## 305 **Conclusion**

306 The switchable phase transformation of Li<sub>2</sub>SO<sub>4</sub> samples from amorphous-glassy-  
307 crystalline-amorphous phase under the influence of dynamic shock wave is reported for the first  
308 time. The observed switchable nature is due to the orientational order-disorder processes  
309 occurring in Li<sub>2</sub>SO<sub>4</sub> specimen. Under the influence of shock wave, the position of the mobile Li  
310 atom changes which is reflected in the post-shock measurements such as XRD, UV-Visible and  
311 Raman spectral studies. The interesting switchable phase transition behavior of Li<sub>2</sub>SO<sub>4</sub> has been  
312 authentically demonstrated by crystallographic, optical and vibrational spectroscopic techniques.  
313 Among the listed shock wave induced phases of the test sample, glassy phase has higher  
314 electrical conductivity because of the presence of higher mobility of lithium ions based on peddle  
315 –wheel mechanism. It is firmly believed that the present approach could be the starting point  
316 which may trigger the pathway to find many more materials of possible reversibility occurring at  
317 shocked conditions i.e., from amorphous to crystalline nature and vice versa. From the observed  
318 results, it is very realistic that Li<sub>2</sub>SO<sub>4</sub> sample has the suitability for the applications of phase –  
319 change memory, sensors, molecular switches, pressure transmitters and thermal energy storage  
320 devices. The investigations on the electrical conductivity and magnetic properties of the control  
321 and shocked Li<sub>2</sub>SO<sub>4</sub> samples are under progress.

322 **Compliance with ethical standards**

323 None

324 **Conflict of interest**

325 The authors declare that they have no conflict of interest.

326 **Acknowledgement**

327 The authors thank Department of Science and Technology (DST), India for funding through  
328 DST-FIST programme (SR/FST/College-2017/130 (c)) and Abraham Panampara Research  
329 Fellowship.

330 The project was supported by Researchers Supporting Project number (RSP-2021/231), King  
331 Saud University, Riyadh, Saudi Arabia.

332

333 **References**

334 [1] Bhattacharyya, S.; Maity, M.; Chowdhury, A.; Saha, M.L.; Panja, S.K.; Stang, P.J.; and  
335 Mukherjee, P.S. Coordination-Assisted Reversible Photoswitching of SpiropyranBased  
336 Platinum Macrocycles. *Inorg. Chem.* **2020**, *59*, 2083–2091.

337 [2] Yang, L.; Xiu-Ni, H.; Wei-Qiang, L.; Ji-Xing, G.; Zi, Y. A room temperature reversible  
338 phase transition containing dielectric switch of a host-guest supramolecular metal-halide  
339 compound. *Dalton Trans.*, **2017**, *46*, 12760-12765.

340 [3] Hu, J.; Ichianagi, K.; Takahashi, H.; Koguchi, H.; Akasaka, T.; Kawai, N.; Nozawa, S.;  
341 Sato, S.; Sasaki, Y.C.; Adachi, S.; and Nakamura, K.G. Reversible phase transition in  
342 laser-shocked 3Y-TZP ceramics observed via nanosecond time-resolved x-ray  
343 diffraction. *J. Appl. Phys.* **2012**, *111*, 053526.

344 [4] Tang, Y.Z.; Gu, Z.F.; Yang, C.S.; Wang, B.; Tan, Y.H.; and Wen, H.R. Unusual Two-  
345 step Switchable Dielectric Behaviors and Ferroelastic Phase Transition in a Simple 18-  
346 Crown-6 Clathrate. *Chemistry Select* **2016**, *1*, 6772–6776.

- 347 [5] Machon, D.; Meersman, F. ; Wilding, M.C.; Wilson, M.; McMillan, P.F. Pressure-  
348 induced amorphization and polyamorphism: Inorganic and biochemical systems.  
349 *Prog.Mater.Sci.* **2014**, *61*, 216–282.
- 350 [6] Zhang, L.; Wang, J.; Lv, J.; and Ma, Y. Materials discovery at high pressures. *Nat.*  
351 *Rev. Mater.*, **2017**, *2*, 1-16.
- 352 [7] Stefano, B.; Massimo, M.; Gernot, B.; and Fabbiani, F.P.A.; Pressure-Induced  
353 Conformational Change in Organic Semiconductors: Triggering a Reversible Phase  
354 Transition in Rubrene. *J.Phys.Chem.C*, **2014**, *118*, 13476–13483.
- 355 [8] Bennett, T.D.; Simoncic, P.; Moggach, S.A; Fabia, G.; Piero, M.D.A. K.; Tana, J.C.; and  
356 Cheetham, A.K. Reversible pressure-induced amorphization of a zeolitic imidazolate  
357 framework (ZIF-4). *Chem. Commun.* **2011**, *47*, 7983–7985.
- 358 [9] Wang, K.; Jing, L.; Ke, Y.; Bingbing, L.; and Zou, B. High-Pressure-Induced Reversible  
359 Phase Transition in Sulfamide. *J.Phys.Chem.C*. **2014**, *118*, 18640–18645.
- 360 [10] Vegas, A.; Grzechnik, A.; Syassen, K.; Loa, I. ; Hanfland, M.; and Jansen, M.  
361 Reversible phase transitions in Na<sub>2</sub>S under pressure: A comparison with the cation array  
362 in Na<sub>2</sub>SO<sub>4</sub>. *Acta Cryst. B* **2001**, *57*, 151 – 156.
- 363 [11] Koteeswara Reddy, N. ; Jayaram, V.; Arunan, E.; Kwon, Y.B.; Moon, W.J.; Reddy, K.P.J.  
364 Investigations on high enthalpy shock wave exposed graphitic carbon nanoparticles.  
365 *Diamond. Rel.Mater.* **2013**, *35*, 53–57.
- 366 [12] Jayaram, V.; and Reddy, K.P.J. Catalytic Effect of CeO<sub>2</sub>-Stabilized ZrO<sub>2</sub> Ceramics with  
367 Strong Shock-Heated Mono- and Di-Atomic Gases. *J. Am. Ceram. Soc.* **2016**, *99*, 4128–  
368 4136.
- 369 [13] Carli, P.S.D.; Jamieson, J.C. Formation of an Amorphous Form of Quartz under Shock  
370 Conditions. *J.Chem. Phys.*, **1959**, *31*, 1675.
- 371 [14] Su, Z.; Shaw, W.L.; Miao, Y.R.; You, S.; Dlott, D.D.; Suslick, K.S. Shock Wave  
372 Chemistry in a Metal–Organic Framework. *J.Am.Chem.Soc.* **2017**, *139*, 4619–4622.
- 373 [15] Rohan, A.; and Knowles, J.K. On a shock-induced martensitic phase transition.  
374 *J.Appl.Phys.* **2020**, *87*, 1123.

- 375 [16] Sivakumar, A.; Balachandar, S.; Martin Britto Dhas, S. A., Measurement of “Shock  
376 Wave Parameters” in a Novel Table-Top Shock Tube Using Microphones. *Hum.Fact.*  
377 *Mech.Eng. Defen. Safety.* **2020** 4, 1-6.
- 378 [17] Sivakumar, A.; Soundarya, S.; Sahaya Jude Dhas, S.; Kamala Bharathi, K.; and Martin  
379 Britto Dhas, S. A. Shock Wave Driven Solid State Phase Transformation of  $\text{Co}_3\text{O}_4$  to  
380  $\text{CoO}$  Nanoparticles. *J. Phys. Chem. C* **2020**, *124*, 10755–10763.
- 381 [18] Mowlika, V.; Sivakumar, A.; Martin Britto Dhas, S. A.; Naveen, C.S.; Phani, A. R.;  
382 Robert, R. Shock wave-induced switchable magnetic phase transition behaviour of  
383  $\text{ZnFe}_2\text{O}_4$  ferrite nanoparticles. *J Nanostruct Chem.* **2020**, *10*, 203–209.
- 384 [19] Sivakumar, A.; Reena Devi,S.; Sahaya Jude Dhas, S.; Mohan Kumar R.; Kamala  
385 Bharathi, K.; and Martin Britto Dhas, S. A. Switchable Phase Transformation  
386 (Orthorhombic - Hexagonal) of Potassium Sulfate Single Crystal at Ambient  
387 Temperature by Shock Waves. *Cryst.Grwoth.Des.* **2020**, *20*, 7111-7119
- 388 [20] Lemos, V.; and Sergio, C.S. High-pressure phase transitions in  $\text{Li}_2\text{SO}_4$ . *Phys.Rev.B.*  
389 **1990**, *41*, 593- 596.
- 390 [21] Alieva, A. R.; Akhmedova, I.R.; Kakagasanova, M.G.; and Aliev, Z. A. Raman Spectra  
391 of Polycrystalline Lithium Sulfate, Sodium Sulfate, and Potassium Sulfate in the  
392 Pretransition Temperature Range Lower the Structural Phase Transition. *Phys.Solid*  
393 *State.* **2019**, *61*, 1464–1470.
- 394 [22] Enzo, C.; Roger, F. Temperature dependent Raman spectra of monoclinic and cubic  
395  $\text{Li}_2\text{SO}_4$ . *J.Chem.Phys*, **1984**, *81*, 4729.
- 396 [23] Lemos,V. Pressure Induced Transitions in  $\text{Li}_2\text{SO}_4$ . *High.Press.Res* **1990**, *3*, 37-39.
- 397 [24] Karlsson, L.; McGreevy, R.L.; Mechanisms of ionic conduction in  $\text{Li}_2\text{SO}_4$  and  $\text{LiNaSO}_4$ :  
398 Paddle wheel or percolation? *Solid State Ion.* **1995**, *76*, 301-308.
- 399 [25] Mellander, B.E.; and Lazarus; D.; Electrical conductivity and activation volume for  
400  $\alpha\text{-Li}_2\text{SO}_4$ . *Phys.Rev.B.* **1985**, *31*, 6801- 6803.
- 401 [26] Meilander, B.E.; and Nilsson, L. Thermal Expansion of Lithium Sulphate.  
402 *Z. Naturforsch.* **1983**, *38*, 1396- 1399.

- 403 [27] Raul, K.; Nilsson,L.; Hessel Andersen,N.; Lundent,A.; and John,O.T. A single-crystal  
404 neutron diffraction study of the structure of the high-temperature rotor phase of lithium  
405 sulphate. *J.Phys.:Condens.Matter* **1992**,*4*,1925-1933.
- 406 [28] Nord,A.G.; Crystal structure of  $\beta$ -Li<sub>2</sub>SO<sub>4</sub>. *Acta Cryst. B.* **1976**, *32*, 982.
- 407 [29] Lunden, A. On the Paddle -Wheel Mechanism for Cation Conduction in Lithium  
408 Sulphate. *Z.Naturforsch.* **1995**, *50*, 1067-1076.
- 409 [30] Stephen, H. Superionics: crystal structures and conduction processes. *Rep.Prog.Phys.*  
410 **2004**, *67*, 1233–1314.
- 411 [31] Muller, C.R.; Johansson,P.; Karlsson,M.; Maass,P.; and Matic,A.; Structure of glassy  
412 lithium sulfate films sputtered in nitrogen: Insight from Raman spectroscopy and ab initio  
413 calculations. *Phys.Rev B.* **2008**, *77*, 094116.
- 414 [32] Machon, A.; Pinheiro, C.B.; Bouvier, P.; Dmitriev, V.P. ; and Crichton, W.A. Absence  
415 of pressure-induced amorphization in LiKSO<sub>4</sub>. *J. Phys.:Condens.Matter.* **2010**, *22*,  
416 315401.
- 417 [33] Ghosh, C., and Varma, B.P.; optical properties of amorphous and crystalline Sb<sub>2</sub>S<sub>3</sub> thin  
418 films. *Thin Solid Films*, **1979**, *60*, 61-65.
- 419 [34] Ghosh, C.; and Varma, B.P.; Some optical properties of amorphous and crystalline  
420 antimony trisulphide thin films. *Solid.State.Commun*, **1979**, *31*, 683-686.
- 421 [35] Sivakumar, A.; Saranraj, A.; Sahaya Jude Dhas, A.; and Martin Britto Dhas. S.A.  
422 Shock wave induced enhancement of optical properties of benzil Crystal. *Mater. Res.*  
423 *Express.* **2019**, *6*, 046205.
- 424 [36] Alicia, B.; Ming, L.; Frank, B.; and Jim, H. Investigation of Lithium Sulphate for High  
425 Temperature Thermal Energy Storage. *AIP Conf. Proc.* **2016**, *1850*, 1-9.
- 426 [37] Satheesan Babu, C.; Bhalachandra, L.T.; Dynamics in superionic lithium sulphate lattice:  
427 paddle wheel versus percolation mechanism. *Chem.Phys.Lett.* **1992**, *194*, 351-354.
- 428 [38] Andrikopoulos, K.S.; Yannopoulos, S.N.; Voyiatzis, G.A.; Kolobov, A.V.; Ribes, M.;  
429 and Tominaga.T. Raman scattering study of the a-GeTe structure and possible  
430 mechanism for the amorphous to crystal transition. *J. Phys.: Condens. Matter.***2006**, *18*,  
431 965–979.

- 432 [39] Kolobov, A.V.; Krbal, M.; Fons, P.; Tominaga, J.; and Uruga, T. Distortion-triggered  
433 loss of long-range order in solids with bonding energy hierarchy. *Nat.Chem.* **2011**, *3*,  
434 311-316.
- 435 [40] Cazzanelli, E.; and Frech, R., Raman spectra of  $^7\text{Li}_2\text{SO}_4$  and  $^6\text{Li}_2\text{SO}_4$ . *J.Chem. Phys.*  
436 **1983**, *79*, 2615.
- 437 [41] Cazzanelli, E.; and Frech, R.,; Temperature dependent Raman spectra of monoclinic and  
438 cubic  $\text{Li}_2\text{SO}_4$ . *J.Chem. Phys* **1984**, *81*, 4729.
- 439 [42] Muller, C.R.; Johansson, P.; Karlsson, M.; Maass, P.; and Matic, A., Structure of glassy  
440 lithium sulfate films sputtered in nitrogen: Insight from Raman spectroscopy and ab initio  
441 calculations. *Phys.Rev B*, **2008**, *77*, 094116.
- 442 [43] Frech, R.; and Cazzanelli, E. Raman Spectroscopic Studies of  $\text{Li}_2\text{SO}_4$ . *Solid.State.Ionics*,  
443 **1983**, *10*, 95-100.
- 444 [44] Sivakumar, A.; Shailaja, P.; Sahaya Jude Dhas, S.; Sivaprakash, P.; Almansour, A.I.;  
445 Suresh Kumar, R.; Arumugam, N.; Arumugam, S.; Chakraborty, S.; and Martin Britto  
446 Dhas, S.A. Dynamic Shock Wave-Induced Switchable Phase Transition of Magnesium  
447 Sulfate Heptahydrate. *Cryst. Growth Des.* **2021**, *21*, 5050–5057
- 448 [45] Sivakumar, A.; Sahaya Jude Dhas, S.; Sivaprakash, P.; Almansour, A.I.; Suresh Kumar,  
449 R.; Arumugam, N.; Arumugam, S.; and Martin Britto Dhas, S. A.; The switchable phase  
450 transition of sodium sulfate crystals activated by shock waves. *New J. Chem.*, **2021**, *45*,  
451 16529.
- 452 [46] Sakuntala, T.; Arora,A.K.; Chandra Shekar, N.V.; and Sahu, P.C. Pressure-induced  
453 amorphization and orientational disorder in potash alum. *J. Phys.: Condens. Matter*,  
454 **2000**, *12*, 4417–4432.
- 455 [47] Sakuntala, T.; Arora, A. K.; Chandra Shekar, N. V.; and Sahu, P. Ch. Orientational  
456 disorder: A mechanism of amorphization at high pressure. *Europhys. Lett.* **1998**, *44*, 728-  
457 733.
- 458  
459  
460  
461